Cell Reports

Article

Predictability alters information flow during action observation in human electrocorticographic activity

Graphical abstract

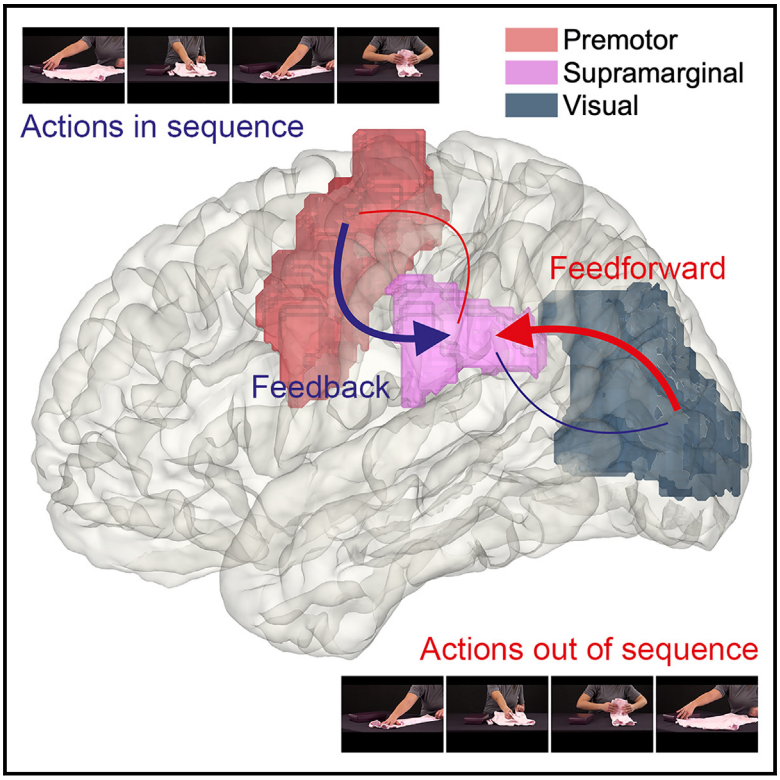

Highlights

- iEEG can track direction of information flow while viewing natural action sequences
- Embedding acts in predictable sequences increase premotor→parietal beta information flow
- The generated expectations suppress broadband gamma activity in occipital cortices
- This supports the notion of predictive coding in the action observation network

Authors

Chaoyi Qin, Frederic Michon, Yoshiyuki Onuki, ..., Pascal Fries, Valeria Gazzola, Christian Keysers

Correspondence

v.gazzola@nin.knaw.nl (V.G.), c.keysers@nin.knaw.nl (C.K.)

In brief

Qin et al. investigate how observing acts in meaningful action sequences alters information flow in the action observation network. They show that embedding acts in predictable action sequences increased top-down beta information flow from premotor regions while suppressing bottom-up gamma information flow from visual areas.

Qin et al., 2023, Cell Reports *42*, 113432
November 28, 2023
https://doi.org/10.1016/j.celrep.2023.113432

CellPress

Cell Reports

CellPress
OPEN ACCESS

Article

Predictability alters information flow during action observation in human electrocorticographic activity

Chaoyi Qin,[1,6] Frederic Michon,[1] Yoshiyuki Onuki,[2] Yohei Ishishita,[2] Keisuke Otani,[2] Kensuke Kawai,[2] Pascal Fries,[3,4] Valeria Gazzola,[1,5,*] and Christian Keysers[1,5,6,*]

[1]Social Brain Lab, Netherlands Institute for Neuroscience, Royal Netherlands Academy of Art and Sciences, 1105 BA Amsterdam, the Netherlands

[2]Department of Neurosurgery, Jichi Medical University, Tochigi 329-0498, Japan

[3]Ernst Strüngmann Institute (ESI) for Neuroscience in Cooperation with Max Planck Society, 60528 Frankfurt, Germany

[4]Donders Institute for Brain, Cognition and Behaviour, Radboud University, Kapittelweg 29, 6525 EN Nijmegen, the Netherlands

[5]University of Amsterdam, Department of Psychology, Brain & Cognition, Amsterdam, the Netherlands

[6]Lead contact

*Correspondence: v.gazzola@nin.knaw.nl (V.G.), c.keysers@nin.knaw.nl (C.K.)

https://doi.org/10.1016/j.celrep.2023.113432

SUMMARY

The action observation network (AON) has been extensively studied using short, isolated motor acts. How activity in the network is altered when these isolated acts are embedded in meaningful sequences of actions remains poorly understood. Here we utilized intracranial electrocorticography to characterize how the exchange of information across key nodes of the AON—the precentral, supramarginal, and visual cortices—is affected by such embedding and the resulting predictability. We found more top-down beta oscillation from precentral to supramarginal contacts during the observation of predictable actions in meaningful sequences compared to the same actions in randomized, and hence less predictable, order. In addition, we find that expectations enabled by the embedding lead to a suppression of bottom-up visual responses in the high-gamma range in visual areas. These results, in line with predictive coding, inform how nodes of the AON integrate information to process the actions of others.

INTRODUCTION

How the brain processes the observed actions of others is a question of enduring interest. The network of brain regions recruited by action observation (action observation network, AON) has been mapped in some detail by having monkeys and humans view isolated actions, typically lasting a couple of seconds, such as grasping or manipulating objects. It includes nodes around the medial occipital, supramarginal, and precentral gyri also activated during the execution of similar actions.[1–3] Outside the laboratory, actions seldom occur as isolated 2-s acts. Instead, individual acts, such as grasping a knife, follow each other in somewhat predictable order within meaningful sequences to achieve an overarching intention, such as preparing breakfast.[4,5] How does the predictability of the acts within such sequences influence how they are processed? How is information integrated across the nodes of the AON, and how does the predictability of an act within a sequence influence this information flow? These questions are at the heart of this study.

That predictions play a key role in perception, and manifest as feedback information flow in the beta band from higher brain regions to lower sensory brain regions, has become prominent in neuroscience.[6,7] In many models of predictive coding or active inference, these feedback predictions are thought to attenuate the response to expected stimuli in lower, visual cortices.[6–8] Empirical evidence of whether such feedback is also increased, and visual representations suppressed, within the AON when acts become predictable remains scarce—despite these features having been at the center of influential models of AON information integration for decades.[9–13]

Evidence that predictions are computed within premotor cortices in the monkey AON comes from single-cell responses depending on what action can be predicted to come next.[14–18] That neural response latencies to predictable observed actions can be shorter in premotor than parietal cortices is compatible with the notion that predictions could be transmitted from premotor to parietal cortices.[19] In the human AON, action-related information in the blood-oxygen-level-dependent (BOLD) response in parietal and premotor cortices depends on the sequence in which acts are presented,[20] and electroencephalogram (EEG) recordings reveal anticipatory activity in the AON when movements are expected.[21] Unfortunately, whether information in fMRI studies flows from premotor to parietal cortices remains unclear, as directional connectivity measures applied to the BOLD signal are notoriously unreliable.[22] Tentative analyses however are encouraging: using Granger causality

measures, participants playing charades seem to send more information from premotor to parietal cortices when guessing the meaning sequences of gestures,[23] and using dynamic causal modeling, seeing people move in unpredictable ways triggers changes in flow in the premotor to parietal direction.[24] Using methods other than traditional fMRI would thus be important to corroborate these findings.

What paradigm should be used? Different paradigms have been developed to study predictions in the visual system. A careful review concluded that the cleanest and most successful strategy has been to contrast different *sequences* of stimuli: if stimuli appear in a highly familiar order, they become *expected*, because their probability is constrained by the preceding stimulus; if they appear in random sequences, they become *neutral*, as their probability is unconstrained by previous stimuli.[8] Comparing responses to expected, neutral stimuli then provide a good measure of the effect of predictions. The term *neutral* differentiates stimuli with a probability that is independent of the prior stimuli from truly *surprising* stimuli, i.e., those occurring if an ordered sequence predicts one stimulus, but a different stimulus is presented. Surprising stimuli trigger attentional processes that are difficult to disentangle from predictions, which is why their use to study predictions has been discouraged.[8] Interestingly, contrasting stimuli in expected vs. random sequences has also been helpful in revealing how cortical networks are altered when words occur in meaningful sentences using fMRI and electrophysiological measures,[25,26] and this this approach thus appears as a strong candidate to investigate the effect of predictions and their suppressive effects also in the AON. As lessons learned from visual neuroscience have led to the conclusion that "experiments testing for ES (expectation suppression) should employ a range of recording techniques under similar or identical stimulation conditions"[8] and that "time-resolved electrophysiological measures may be especially useful,"[8] one should ideally perform such experiments using a variety of recording modalities, including EEG, traditional 3T fMRI, depth-resolved 7T fMRI, and intracranial electrocorticography (ECoG).

Accordingly, we recorded a number of longer action sequences that should be familiar to most participants (Figure 1; Table 1), and we aimed to present them to participants in two forms: first in their intact, natural order, in which each act can be expected based on the previous acts and our decade long experience with these actions, and second, in a scrambled order, in which the same individual acts are relatively neutral, i.e., their probability is only minimally constrained by the previous acts. As simply cutting movies at the transition between consecutive acts and randomizing the sequence would introduce sudden visual changes in the scrambled sequence that are absent in the intact sequence, we recorded the sequences with two cameras 45° apart, and we alternated between the two views between acts in both the intact and scrambled sequences. This ensured similar levels of visual transients in both conditions (see Figure S1 for a quantification), with the predictability of the individual acts now being the primary difference between the sequences. We then compared intact vs. scrambled sequences using multiple recording methods across multiple studies. Here we present data recorded from intracranial ECoG measurements. Using the same stimuli while recording 3T fMRI revealed that the information content in premotor and parietal cortices was higher for intact sequences, showing that these regions are sensitive to the predictability of observed actions, and while recording EEG, that responses in electrodes over the occipital lobe were suppressed in the intact sequences, in line with the notion of expectation suppression.[20] Whether the information flow was increased in the premotor to parietal direction for intact sequences could not be determined due to the limitations of the methods. Using these stimuli while measuring BOLD activity in a depth-resolved 7T fMRI study, we leveraged that feedback connections from premotor to inferior parietal regions are known to terminate in layers 3, 5, and 6 in the monkey, and we found that information was indeed increased at depths aligning with these layers in the intact − scrambled contrast, and intersubject functional connectivity confirmed that this effect could originate from premotor feedback.[27]

As attributing BOLD activity at certain depths to feedback or feedforward information remains tentative, particularly outside of the visual cortices,[28] here we aim to leverage the unique properties of ECoG to provide independent evidence by leveraging the observation that feedforward information flow associated with visual input and the feedback information flow associated with predictions are associated with directed information transfer in distinguishable frequency bands, namely the gamma and beta band, respectively.[6,29,30] Both the gamma and the beta bands contain separable subbands with distinct functions.[31,32] Between the premotor and parietal lobes, the high-gamma (60–90 Hz) and high-beta (20–30 Hz) frequency bands seem particularly relevant to information integration,[33,34] and these bands will therefore be our frequency ranges of interest. We expect two effects when comparing expected versus neutral acts using the intact versus scrambled sequence contrasts: First, that the parietal node of the AON, in the supramarginal gyrus (SMG) should receive more premotor feedback from the precentral gyrus (PreCG) in the high-beta range for intact than scrambled sequences, and second, that visual response in the high-gamma band should be suppressed in the visual node of the AON in the middle occipital gyrus (MOG) for this intact compared to the scrambled sequences (Figures 1A and 1B). We thus selected ECoG electrodes in the precentral, supramarginal cortex and MOG across 10 patients implanted with ECoG grids (Figure 1C). We selected those three regions because they encompass key nodes of the AON and because we had a sufficient number of patients with ECoG strips that encompassed pairs of these regions to calculate measures of directed information transfer: seven patients had electrodes in the PreCG and SMG and six had electrodes in the SMG and MOG (Figure 1D).

RESULTS

Increased high-beta power in precentral and supramarginal channels for expected actions

To investigate whether beta oscillations were indeed increased for expected action sequences, as an increase in feedback information may suggest, we calculated the power spectral density for all movies in each condition and used a linear mixed effect model (LME) to compare power across conditions. We found that in the high-beta range, precentral and supramarginal regions showed the hypothesized increase in power for the more

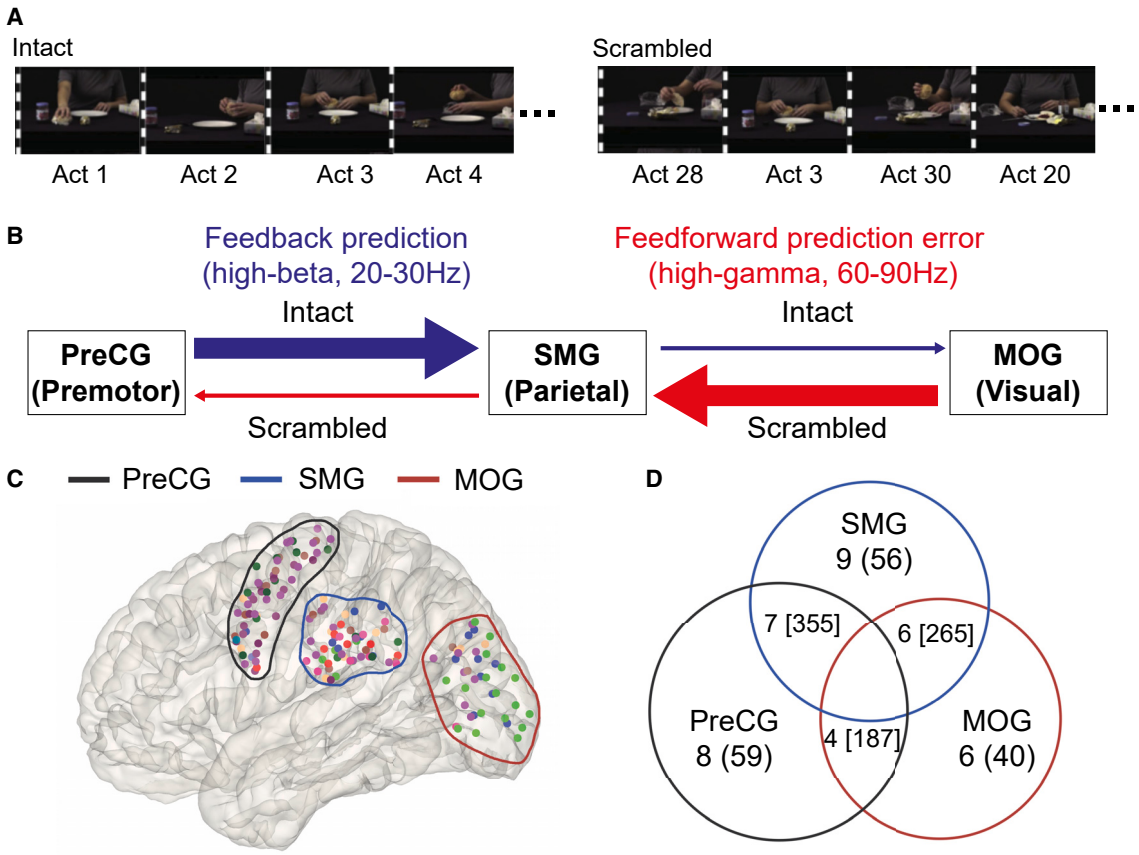

Figure 1. Stimuli and hypotheses

(A) We presented participants with movies of everyday hand actions lasting ~1 min in length, filmed simultaneously with two cameras 45° apart, which were cut into ~30 individual motor acts lasting ~2 s (Table 1). In the intact condition, the motor acts were presented in their original order but switching from one camera view to the other at the transition between acts to introduce visual transients similar to those in the scrambled condition. In the scrambled condition, the acts were presented in randomized order.

(B) We hypothesize that for intact sequences (top arrows), the parietal node of the action observation network in the supramarginal gyrus (SMG) would receive comparatively more feedback information (blue) from the premotor nodes in the precentral gyrus (PreCG) than for scrambled sequences (bottom arrows). We further hypothesized that for intact sequences, responses to the expected acts would be suppressed in the visual cortices in the middle occipital gyrus (MOG) compared to the scrambled condition. Accordingly, feedforward visual information (red arrows) would be more prevalent in the scrambled sequences (bottom arrows). We expect feedforward information to be mainly in the gamma range (60–90 Hz) and feedback signals to be mainly in the high-beta range (20–30 Hz); the size and direction of the arrows represent the relative strength of coherence and PSI, respectively.

(C) The spatial distribution of electrodes in the three regions on a glass brain in MNI space; the colored circles depict the rough boundaries of these regions.

(D) The numbers outside the parentheses represent the number of patients who have electrodes in this region or across two regions. The numbers inside the parentheses represent the total number of recording electrodes in this region. The numbers inside the square brackets represent the total number of recording electrode pairs across two regions.

expected, intact compared to the scrambled condition ($p < 0.05$, corrected) (Figures 2A and 2B). When we averaged the power at the hypothesized high-beta frequency range (20–30 Hz) in each person across all electrodes, we saw that the majority of subjects had higher beta power in the intact condition, in both the precentral (LME, $t_{(116)} = 3.09$, $p = 0.002$) (Figure 2A, inset left) and the supramarginal region (LME, $t_{(110)} = 2.29$, $p = 0.02$) (Figure 2B, inset left).

Reduced gamma power in middle occipital channels for expected actions

To investigate the notion that expected actions show suppressed feedforward signals in the gamma range in earlier visual cortices, we quantified the power in the gamma range. We observed opposite effects in earlier visual cortices and supramarginal cortices. We found the hypothesized reduction of gamma power for the expected, intact movies compared to the scrambled movies in channels over the middle occipital cortices ($p < 0.05$, Figure 2C). However, over the supramarginal cortices, we found significantly higher gamma power in intact compared to scrambled condition ($p < 0.05$, Figure 2B). Examining the averaged power in the gamma band (60–90 Hz), we found that most of the participants had higher gamma power in the intact condition in the supramarginal (LME, $t_{(110)} = 3.12$, $p = 0.002$) (Figure 2B, inset right) but higher gamma power in the scrambled condition in the middle occipital cortices (LME, $t_{(78)} = -2.64$, $p = 0.01$) (Figure 2C, inset right).

Table 1. Stimuli

	Action	Seconds	Acts
1	inflating and tying a balloon	51	27
2	preparing bread with butter and jam	79	40
3	sewing a button	66	42
4	writing a gift card	83	39
5	arranging flowers in a vase	82	39
6	framing a picture	112	39
7	cleaning spectacles	69	38
8	cleaning a laptop screen	46	28
9	sending a letter	42	34
10	replacing battery in a torch	51	27
11	replacing a pillow cover	44	35
12	folding a shirt	38	20
a	toasting bread	65	30
b	making a paper boat	94	32
c	rolling a cigarette	72	30
d	applying nail polish	49	23
e	squeezing oranges	62	40
f	sharpening a pencil.	83	44
g	removing nail polish	64	32
h	preparing a sandwich	77	27

List of sequences used as stimuli with total duration in seconds and number of motor acts shown. The first 12 were rated as familiar to Japanese individuals based on an informal evaluation by experimenter Y.O. The remaining 8 (labeled with letters a–h) from the original study by Thomas et al.[20] were not used, because they were considered less familiar to Japanese individuals.

Temporal dynamics of beta and gamma power relative to camera change

We next investigated the temporal dynamics of both high-beta and -gamma power in these regions just before and after the camera changes. The camera changes represent a challenging event for the brain. From a low-level visual point of view, camera changes lead to a sudden change in the visual input (Figure S1), similar to those occurring during saccades though not self-initiated like saccades. During saccades, predictions from higher-visual areas are thought to maintain a sense of continuity in the visual scene. We may thus expect an interplay between putatively predictive signals in the high-beta range preparing the system for a camera change ramping up around the likely time of a camera change, followed by a high-gamma signal starting in the occipital regions caused by the strong change in visual input following the camera change. The former might be more pronounced for intact sequences and the latter for scrambled sequences.

In the high-beta range, all regions showed a pattern in which power was higher around the time of the camera change than in the middle of a segment. As expected, for precentral and supramarginal channels, the power was higher for the intact sequences, which encourage predictions, at several time points ($p < 0.05$, Figures 3A–3C), with significantly higher beta power in the precentral area from 140 ms before the camera change until 220 ms after the camera change and in the supramarginal area from 380 until 740 ms after the camera change (Figures 3A and 3B). The middle occipital cortex however showed a different pattern, with higher high-beta power for intact movies only appearing late in the segment, with early segments showing the opposite pattern (albeit only at uncorrected levels; Figure 3C).

With regard to high-gamma power, the middle occipital cortex showed the expected increase in high-gamma after typical visual latencies, with the power being lower for the intact than scrambled sequences, as expected if expectation suppression was at play within the AON (Figure 3F). The supramarginal and precentral cortices failed to show such a high-gamma peak following the sudden change in visual input and instead showed a dip in high-gamma power, which in the supramarginal cortex was more pronounced for the scrambled sequences (Figure 3E). Precentral channels, on the other hand, showed no such changes in gamma power (Figure 3D).

Beta synchronization and information transfer between precentral and supramarginal

The increased high-beta activities in precentral channels for intact sequences preceded that in supramarginal channels. This would be in line with a model in which predictions in premotor regions would be transferred backward to the parietal nodes of the AON and in line with single-cell recordings in monkeys.[19] To test this notion, we computed the interregional connectivity across precentral and supramarginal channels using spectral coherence.

First, we measured imaginary coherence (see STAR Methods) using all electrode pairs within the first second after the camera change, and we found significantly higher beta coherence between precentral and supramarginal channels in the intact compared to the scrambled condition. This effect was restricted to the high-beta range (23–30 Hz, $p_{corr} < 0.05$) (Figure 4A). Interestingly, the low-beta range showed a difference in the opposite direction, confirming the functional dissociation between low and high beta.[31] Frequencies around 50 Hz were masked out due to line noise contaminating the coherence estimates. Furthermore, using a sliding window method to characterize the timing of the differential high-beta coherence, we find that it emerges 300 ms after the camera change ($p < 0.05$) (Figure 4C).

To further investigate the directionality of information transfer between the precentral and supramarginal, we calculated the non-parametric Granger causality (GC) using all electrode pairs within the first second after the camera change. In the intact compared to the scrambled condition, the GC spectrum exhibited higher feedback information from precentral to supramarginal in the high-beta band ($p < 0.05$; Figure 5A), but there was no difference between conditions in the opposite (feedforward) direction (Figure 5B). Both GC and coherence exhibited frequencies that were in the high-beta range (20–30 Hz). We estimated the phase slope index (PSI) in 20–30 Hz using a sliding window method to further validate the information flow between precentral and supramarginal in this high-beta range. Starting 400 ms before the camera change, the PSI exhibited opposing information directions, with feedforward information from supramarginal to precentral in scrambled movies and feedback information from precentral to supramarginal in intact movies (Figure 6A).

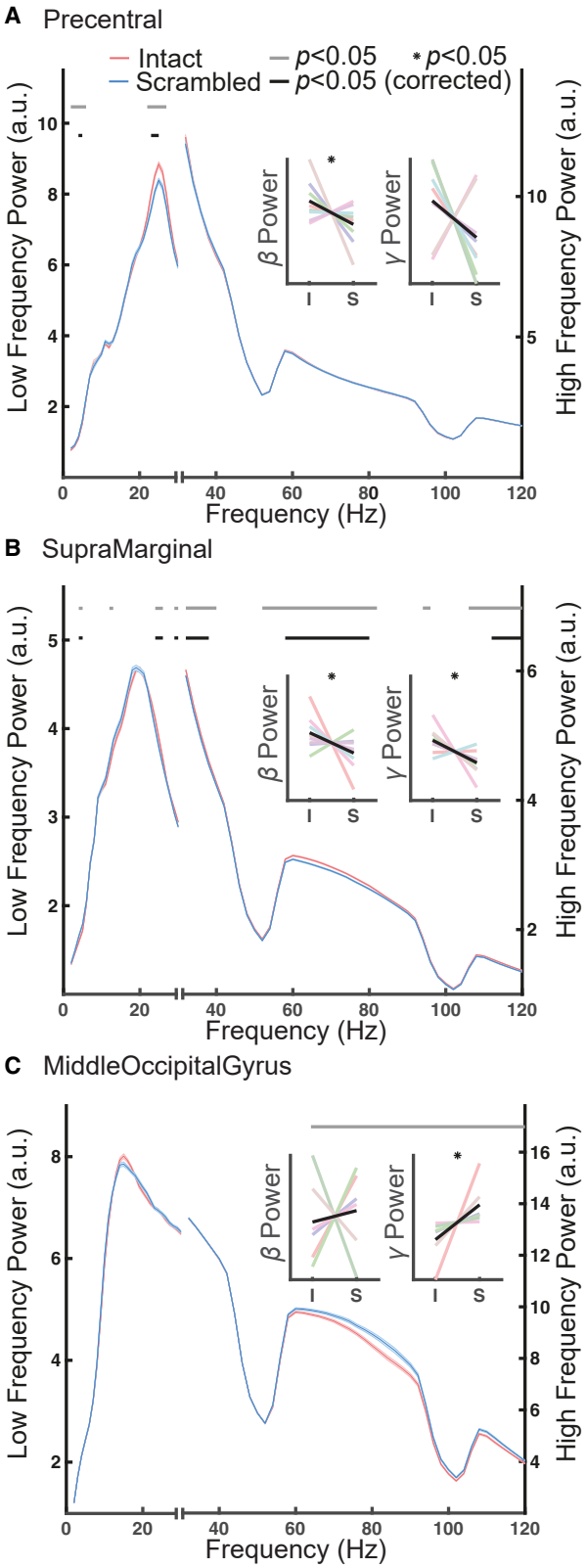

Figure 2. Power spectral density

The power spectral density functions are estimated separately for the low- and high-frequency range across the whole movie viewing period for the intact (red) and scrambled (blue) conditions. The power is shown as power× frequency^2 for illustration. The inserts show the average power over the high-beta (20–30 Hz) and high-gamma (60–90 Hz) range separately for each participant (color) and their average (black) separately for the intact (I) and scrambled (S) condition.

(A) Precentral channels showed significantly higher power in intact conditions from 23 to 25 Hz (LME, n = 59, false discovery rate (FDR) corrected $p < 0.05$) and a similar trend was observed in beta power averaged from 20 to 30 Hz (LME, $t_{(116)} = 3.09$, $p = 0.002$, inset on the left).

(B) Supramarginal channels showed significantly higher power in intact condition from 24 to 26, 29 to 30, 58 to 80, and 112 to 120 Hz (LME, n = 56, FDR corrected $p < 0.05$), and a similar effect was also observed in beta power averaged from 20 to 30 Hz (LME, $t_{(110)} = 2.29$, $p = 0.02$, inset on the left) as well as gamma power averaged from 60 to 90 Hz (LME, $t_{(110)} = 3.12$, $p = 0.002$, inset on the right).

(C) Middle occipital channels showed significantly higher power in scrambled conditions from 64 to 120 Hz (LME, n = 40, uncorrected $p < 0.05$), and the same effect was observed in gamma power averaged from 60 to 90 Hz (LME, $t_{(78)} = -2.64$, $p = 0.01$, inset on the right). Data are presented as mean ± SEM; n represents number of electrodes (A–C).

Gamma synchronization and information transfer between supramarginal and middle occipital cortices

We also looked at the interregional relationships between the supramarginal and middle occipital channels. In both the high-gamma (60–90 Hz) and low-gamma (30–40 Hz) ranges, the computed imaginary coherence during the first second following the camera change indicated significantly stronger gamma coherence between supramarginal and middle occipital channels in the scrambled condition ($p < 0.05$, Figure 4B). Furthermore, the time-resolved coherence increased 400 ms after the camera changed in the scrambled condition ($p < 0.05$, Figure 4D).

Comparing the two conditions using GC did not demonstrate a preferential information direction between supramarginal and middle occipital channels in the gamma band (at $p < 0.05$, Figures 5C and 5D). However, the PSI derived at a high-gamma frequency (60–90 Hz) suggested the expected direction of effect, with reduced feedforward information from the middle occipital to the supramarginal channel, beginning 200 ms after the camera change ($p < 0.05$), for the intact than scrambled condition. (Figure 6B).

DISCUSSION

Our study aimed to provide insights into how the nodes of the AON interact with each other, and how that interaction is altered when acts are not studied in isolation, but in natural sequences in which they can be predicted from the preceding acts. We compared these natural sequences, in which acts could be expected, against a control condition in which the order was randomized to reduce expectations to a neutral level. We found that signals in the high-beta and high-gamma range across the precentral, supramarginal, and middle occipital regions of the AON were indeed differentially modulated by this manipulation. In what follows, we will discuss changes in these two frequency bands separately, together with some background on how

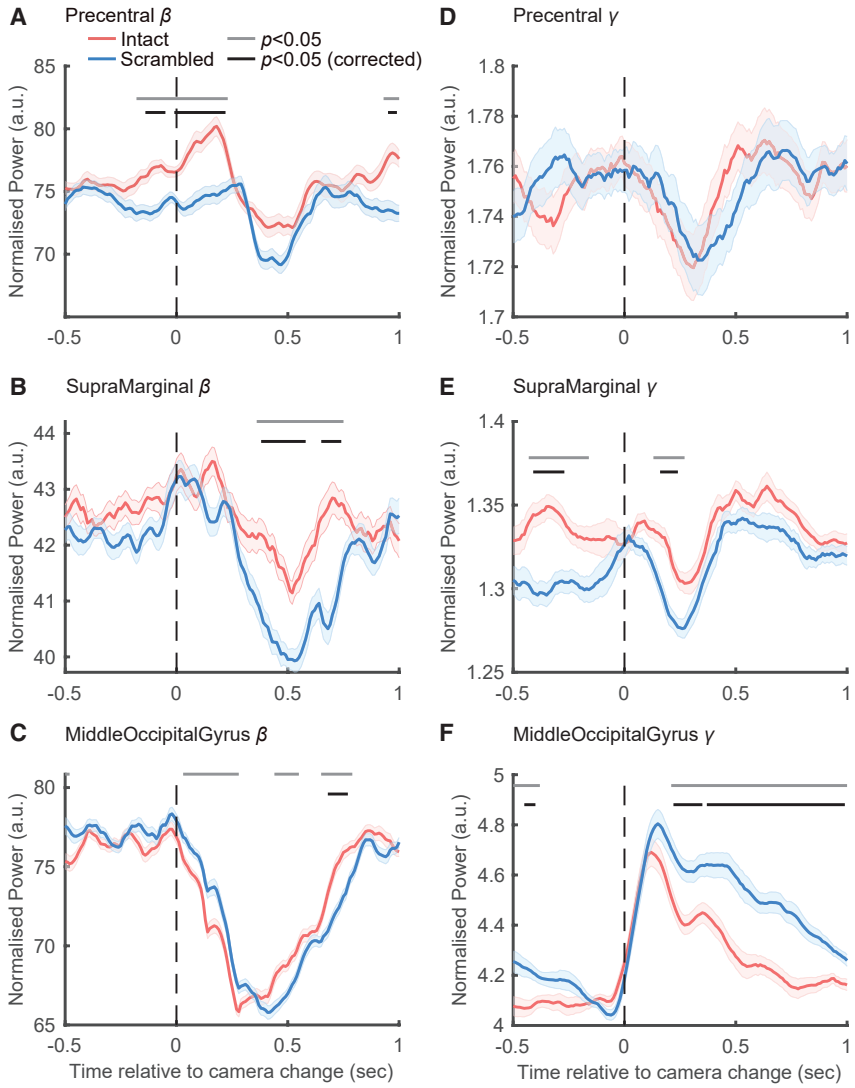

Figure 3. Temporal dynamics of beta and gamma power

Time courses of averaged beta (20–30 Hz, left column) and gamma (60–90 Hz, right column) power in intact (red lines) and scrambled (blue lines) conditions in each region.

(A) Precentral showed significantly higher beta power in intact condition even 140 ms before camera changes, which lasted till 220 ms after the camera changes.

(B) Supramarginal showed significantly higher beta power in intact condition from 380 ms after the camera change.

(C) Middle occipital showed significantly higher beta power in intact condition from 680 ms after the camera change.

(D) Precentral showed no gamma power difference between conditions.

(E) Supramarginal showed significantly higher gamma power in intact condition from 410 ms before and 160 ms after the camera change.

(F) Middle occipital showed significantly reduced gamma power in intact condition from 220 ms after the camera change. Data are presented as mean ± SEM; n represents number of electrodes. Differences between conditions are tested using linear mixed effect models (A–F).

changes in these frequency bands have been associated with feedback and feedforward information flow in the literature.

Beta oscillations in high-level brain regions have been associated with top-down processing and sensori-motor integration via feedback information flow across distal brain regions.[29,30,35–37] Several studies have shown that the power in the beta range, particularly in the high-beta range from 20 to 30 Hz, is modulated by action observation, confirming that it may be important for feedback processes also during action observation.[38–41] Here we found that observation of actions in predictable order caused higher high-beta power in, and higher high-beta coherence between, precentral and supramarginal cortices. While the fact that this power and coherence increase occurs in the beta range is indicative of a feedback direction of information flow, the high temporal resolution of ECoG, and its relatively higher spatial resolution compared to scalp recordings, allows us to directly test the prevalent direction of information flow using phase slope indices and GC. Both methods confirmed that intact sequences lead to more information flow in the high-beta range in the feedback direction from precentral to supramarginal cortices. This provides evidence that the predictability of action sequences indeed increases feedback information, in line with the influential notion of predictive coding during action observation[9,10,12,42] and in line with our findings of increased action-observation-related activity for predictable actions in layers of the SMG known to receive premotor feedback.[43] It has been argued that corroborating findings regarding the effect of expectations using multiple modalities is essential.[8] It is therefore reassuring that these results from ECoG and depth-resolved fMRI using the same stimuli also align with findings using different methods. Monkey single-cell physiology has shown that neurons in the premotor cortex can indeed show anticipatory responses while witnessing the actions of others, in line with a role in generating expectations,[15–18] and the responses in the premotor cortex to such expected action observation at the population level precede those in the parietal cortex, in line with the notion that the predictions could be transmitted from the premotor to the parietal cortices.[19] This finding also dovetails with findings using conventional 3T BOLD measurements that have shown that when participants actively try to guess the meaning of sequences of gestures, GC analyses reveal a net direction of information flow from the premotor to the parietal cortices,[23] and that activity in the premotor and parietal cortices depends on the order in which the acts are presented.[20] That the premotor to parietal connection is influenced by predictability is also in line with a recent finding, using DCM, that effective connectivity in that

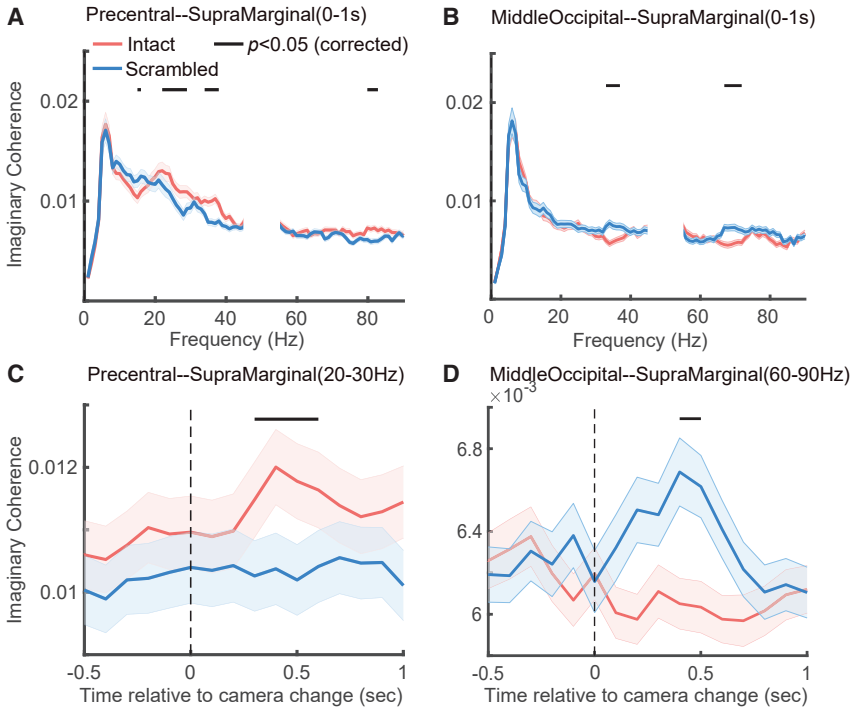

Figure 4. Spectral coherence and temporal dynamics of coherence

(A) Precentral and supramarginal showed significantly higher coherence in intact condition in beta frequency from 23 to 30 Hz (LME, n = 355, FDR corrected $p < 0.05$).

(B) Middle occipital and supramarginal showed significantly higher coherence in scrambled condition in gamma frequency from 68 to 73 Hz (LME, n = 265, FDR corrected $p < 0.05$).

(C) Precentral and supramarginal showed significantly higher coherence in intact condition from 300 ms after camera change (LME, n = 355, FDR corrected $p < 0.05$).

(D) Middle occipital and supramarginal showed significantly higher coherence in scrambled condition from 400 ms after camera change (LME, n = 265, FDR corrected $p < 0.05$). Data are presented as mean ± SEM; n represents number of electrode pairs (A–D).

direction is sensitive to mismatches between expected and observed action kinematics.[24] We observed differences in power across conditions in the high-beta range (20–30 Hz), as expected, and comparing power across all frequencies confirmed that this effect was restricted to the high-beta (>20 Hz) and absent in the low-beta (13–20 Hz) band. The specific role of subbands in the beta range remains incompletely understood,[31] but our findings converge with a small number of studies pointing toward a particular relevance of high beta for integration of motor signals[33,34] and showing that the high-beta range is selectively altered during the observation of other people's actions.[41] Only when examining the coherence between PreCG and SMG across all frequencies did we observe a significant difference in the low-beta range across the intact vs. scrambled condition, and this difference was no longer significant when using GC. Altogether, this confirms the notion that different subbands of beta have different functions, with high beta most involved in top-down effects.[31,32]

Gamma power, in contrast, has been associated with local processing[44] and feedforward information flow.[29,38,45,46] In the visual system, gamma is triggered particularly by sudden changes in the visual input.[47,48] In accordance with that literature, the camera changes, which trigger a sudden change in visual input, triggered a transient in high-gamma power in our more classically visual channels in the MOG, and, perhaps unsurprisingly, such camera-change-locked increases were not observed in the SMG and PreCG, where single-cell recordings in monkeys have shown many neurons to generalize their responses over changes in low-level features and viewpoint[49,50] and continue to respond even when critical aspects of the action are occluded.[18] Given the association of activity in the gamma range with visual changes, it is important that we have not simply compared an intact action sequence without camera changes with its scrambled counterpart, as they would have differed significantly in terms of abrupt visual changes. Instead, by introducing camera changes in both sequences, we have introduced similar levels of pixel-value changes at the transition between acts in both types of sequences (see Figure S1). We had hypothesized that visual responses to the acts would be suppressed in our MOG contacts, based on the expectation suppression reported in other domains of visual neuroscience,[8] and this hypothesis was confirmed: in the intact condition, occipital channels had reduced high-gamma power compared to the scrambled condition. Considering the aforementioned association of high-gamma activity with feedforward visual[45,46,51] and local information,[52,53] this attenuated high-gamma power in the middle occipital cortices suggests, in line with some predictive coding accounts, that expectation suppressions also occur in the visual nodes of the AON. Importantly, we also found the coherence to be reduced in the intact condition across the middle occipital cortex and the SMG, and the PSI confirms that this information in the high-gamma band indeed flowed from the middle occipital to the SMG, in accordance with the notion that visual input to the parietal AON nodes is indeed attenuated by expectations. This expectation suppression dovetails with our EEG finding, using the same stimuli, that showed attenuated responses over the occipital cortex in the intact compared to the scrambled sequences. Considering the different timing of the responses in PreCG and MOG, our results also dovetail with the idea that high-level abstract stimulus features are anticipated earlier than the low-level visual features that are predicted in closer proximity to the actual sensory input.[54]

Interestingly, high-gamma activity in the SMG was increased in the intact compared to the scrambled condition. Given that broadband high-gamma power is known to be tightly linked to neural spiking and thereby reflects local processing,[53] this

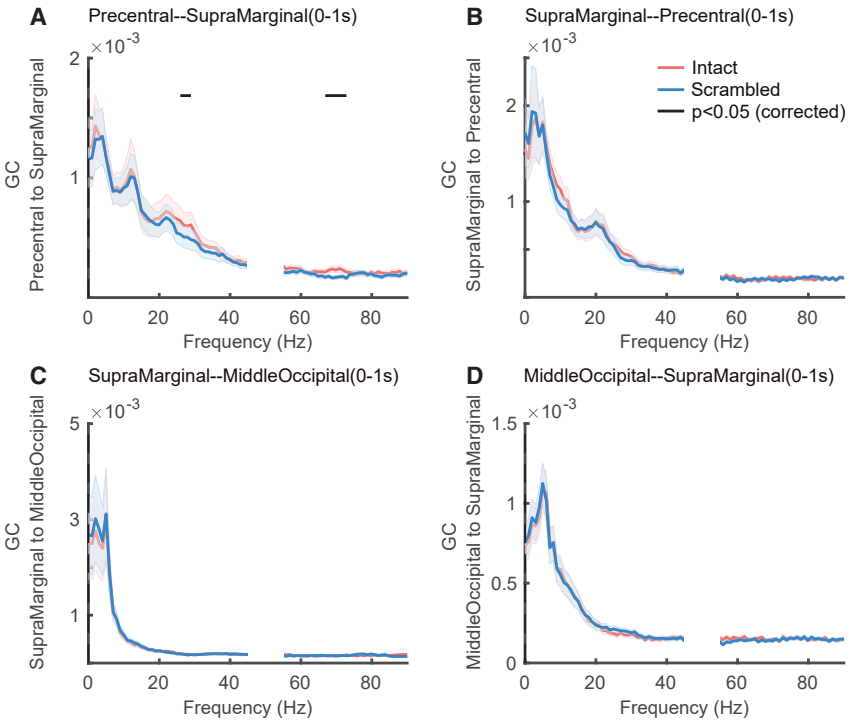

Figure 5. Non-parametric Granger causality

(A) Stronger Granger causality was found from precentral to supramarginal in the intact condition in the beta frequency from 26 to 29 Hz (LME, n = 355, FDR corrected $p < 0.05$).

(B) No significant difference between conditions was found from supramarginal to precentral.

(C and D) No difference was found between middle occipital and supramarginal channels between conditions. Data are presented as mean ± SEM; n represents number of electrode pairs (A–D).

increased high-gamma power in the supramarginal cortex during intact sequences, together with the increased intersubject correlation for intact sequences in the SMG in fMRI BOLD signals,[20] suggests that the parietal node indeed represents more than the individual motor acts that are identical across the intact and scrambled movies, and it preferentially encodes actions when they integrate into larger, meaningful sequences. Such preferential encoding of longer chains of actions in the parietal node contrasts with the expectation suppression that appears to dominate the occipital node, in line with the notion that there is a progressive increase in the "temporal receptive field" of cortical regions along a hierarchy from earlier sensory regions, with activity that integrates information over short intervals to more anterior parietal and frontal regions that can integrate information over minutes.[20,25]

Leveraging the temporal resolution of electrical recordings, and the spatial specificity afforded by recording so close from the cortex, our data therefore add independent evidence for how the brain processes actions when we observe them in larger, meaningful sequences: when predictions are possible (in our intact sequences), feedback information is transmitted in high-beta oscillation from precentral to supramarginal cortices, and local processing in the high-gamma band is increased in the supramarginal cortices and reduced in occipital visual cortices. When expectations are more difficult, as is the case following a camera change in our scrambled sequences, a more prominent transient increase in high-gamma activity in the visual cortices is triggered, and information flows from these visual cortices to the SMG in the gamma band. Zooming in on the moment of a camera change, our data suggest a particular succession of events. For intact sequences, precentral cortices generate high-beta activity thought to reflect predictions just before the camera change, and this increased high-beta activity continues after the camera change. This pattern is reminiscent of the predictive activity around a saccade onset in frontal eye fields that is thought to provide the brain with a continuity of perception despite the low-level discontinuity that a saccade causes.[55,56] In contrast, when visual input is difficult to predict, after a camera change in the scrambled sequences, a more prominent, high-gamma transient, occurring around the typical response latency of visual areas after the camera change, appears to emphasize the transfer of visual information in a forward direction of information flow to the parietal node.

Limitations of the study

Our study has a number of limitations that should be considered. First, we used a passive action observation paradigm. We chose this paradigm because the length of these stimuli (~1 min), and the possibility to use the same stimuli in all participants, allowed us to characterize the effect of expectation in the AON using complementary neural activity recording modalities including faster electrophysiological measurements (EEG and ECoG) and slower traditional and depth-resolved BOLD fMRI. Combining these modalities using the same stimuli avoids that findings are biased by the limitations of a given measurement modality,[8] such as the disrupting effect of variability in hemodynamic responses delays in connectivity analysis in traditional BOLD MRI,[22,57] uncertainty about the attribution of signals at a specific depth or frequency band to feedforward or feedback information in depth-resolved ultra-high field MRI[28] or electrophysiological signals.[58] However, given that perception is ultimately at the service of action, an important complementary approach will be to examine whether the same principles apply when paradigms are more interactive,[59] even if doing so will limit the ability to leverage such a comprehensive range of recording modalities. Second, we focused on three key regions within the AON, while the action observation process is known to be more complex, also involving for instance somatosensory, cerebellar, and other subcortical regions.[1,2,20,60] Future studies involving patients with a wider coverage may be ideally suited to investigate how information from these other nodes may integrate

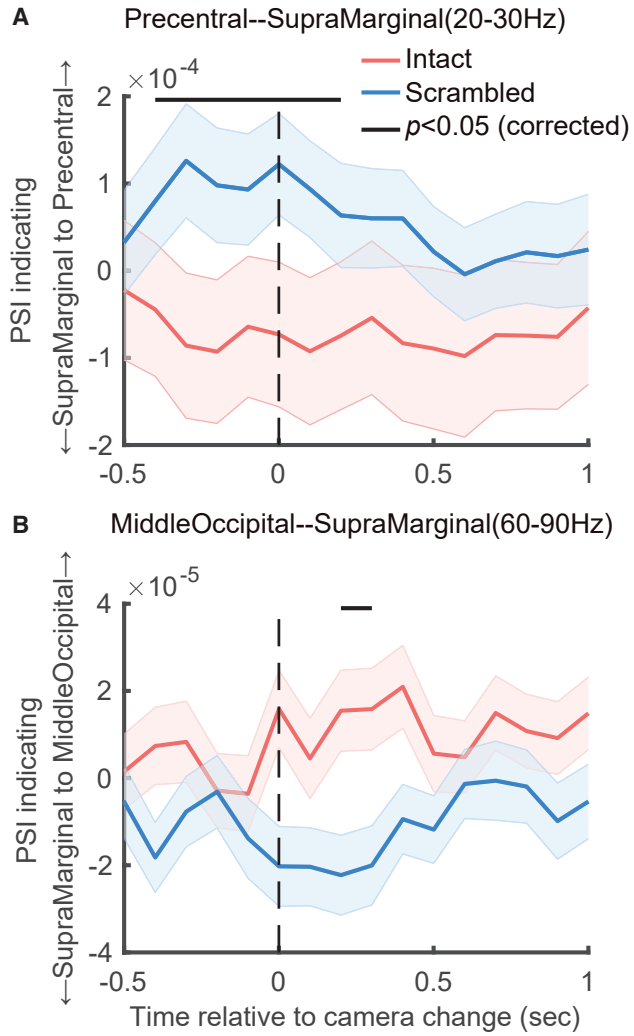

Figure 6. Phase slope index

(A) Phase slope index revealed more beta information (20–30 Hz) from precentral to supramarginal in intact condition but from supramarginal to precentral in scrambled condition (LME, n = 355, FDR corrected $p < 0.05$).

(B) On the other hand, gamma information (60–90 Hz) was observed to transfer more from middle occipital to supramarginal in scrambled condition but from supramarginal to middle occipital in intact condition (LME, n = 265, FDR corrected $p < 0.05$). Data are presented as mean ± SEM; n represents number of electrode pairs (A and B).

with those of the network we focus on. Third, to increase the statistical power of our analyses, we pooled electrodes over relatively large regions of the cortex within our three regions of interest. Future studies may wish to explore whether specific subregions show different patterns. Indeed, some studies mentioned a specific topological organization of the premotor cortex and its connectivity with the parietal lobe in action observation.[24,61] A preliminary analysis of our data however failed to reveal a specific topography of connectivity (Figure S2). Forth, while for the high-beta analysis, two methods estimating the direction of information flow (PSI and GC) agree, for the high-gamma frequency range across the occipital and parietal channels, the PSI analysis revealed a significant difference between conditions, while the GC did not. The exact source of this discrepancy is difficult to identify. It has been suggested that PSI is a more robust and sensitive method than GC when signals contain a mixture of several independent sources and when noise levels are higher.[62–66] The fact that high-gamma frequencies capture more local signals than high-beta frequencies and the large size of our occipital region may have conspired to generate the heterogeneity of signals that GC is thought to suffer from more than PSI. That high-gamma frequencies also have lower power than high-beta frequencies may have additionally increased the relative noise level that GC is thought to suffer from more than PSI. Together this may explain why only the PSI analyses could detect the hypothesized condition effects in the high-gamma signals. Such discrepancy should however temper the confidence we can have in the effect of predictability on the directionality of the information transfer in the gamma band across these regions[67,68] until future studies can better isolate the origins of this discrepancy.

STAR★METHODS

Detailed methods are provided in the online version of this paper and include the following:

- KEY RESOURCES TABLE
- RESOURCE AVAILABILITY
  - Lead contact
  - Materials availability
  - Data and code availability
- EXPERIMENTAL MODEL AND STUDY PARTICIPANT DETAILS
  - Ethics
  - Participants
- METHOD DETAILS
  - Stimuli and experiment procedure
  - Electrophysiological recordings and signal preprocessing
  - Electrode locations and region definition
  - Trial separation
- QUANTIFICATION AND STATISTICAL ANALYSIS
  - Power spectral density
  - Coherence
  - Phase slope index
  - Granger causality
  - Statistical assessment

SUPPLEMENTAL INFORMATION

Supplemental information can be found online at https://doi.org/10.1016/j.celrep.2023.113432.

ACKNOWLEDGMENTS

We thank Teresa de Sanctis for help with preparing the stimuli and Rajat Mani Thomas for help with data analysis. Funding: C.K. was funded by VICI grant 453-15-009, V.G. by VIDI grant 452-14-015, and K.K. by JSPS KAKENHI grant numbers JP17H04305 and JP20H03794.

AUTHOR CONTRIBUTIONS

C.K. and V.G. conceived the study, obtained funding, and supervised the analysis of the data. Y.O. acquired the data. Y.I., K.O., and K.K. performed the surgeries. C.Q. and F.M. analyzed the data with supervision and advice from PF. C.Q. and C.K. wrote the first draft of the paper. All authors edited the manuscript.

DECLARATION OF INTERESTS

The authors report no competing interests.

Received: March 27, 2023
Revised: July 27, 2023
Accepted: October 29, 2023
Published: November 14, 2023

REFERENCES

1. Gazzola, V., and Keysers, C. (2009). The Observation and Execution of Actions Share Motor and Somatosensory Voxels in all Tested Subjects: Single-Subject Analyses of Unsmoothed fMRI Data. Cerebr. Cortex *19*, 1239–1255. https://doi.org/10.1093/cercor/bhn181.
2. Caspers, S., Zilles, K., Laird, A.R., and Eickhoff, S.B. (2010). ALE meta-analysis of action observation and imitation in the human brain. Neuroimage *50*, 1148–1167. https://doi.org/10.1016/j.neuroimage.2009.12.112.
3. Rizzolatti, G., and Sinigaglia, C. (2016). The mirror mechanism: a basic principle of brain function. Nat. Rev. Neurosci. *17*, 757–765. https://doi.org/10.1038/nrn.2016.135.
4. Grafton, S.T., and Hamilton, A.F.d.C. (2007). Evidence for a distributed hierarchy of action representation in the brain. Hum. Mov. Sci. *26*, 590–616. https://doi.org/10.1016/j.humov.2007.05.009.
5. Thioux, M., Gazzola, V., and Keysers, C. (2008). Action understanding: how, what and why. Curr. Biol. *18*, R431–R434. https://doi.org/10.1016/j.cub.2008.03.018.
6. Bastos, A.M., Usrey, W.M., Adams, R.A., Mangun, G.R., Fries, P., and Friston, K.J. (2012). Canonical microcircuits for predictive coding. Neuron *76*, 695–711.
7. Friston, K. (2005). A theory of cortical responses. Philos. Trans. R. Soc. Lond. B Biol. Sci. *360*, 815–836. https://doi.org/10.1098/rstb.2005.1622.
8. Feuerriegel, D., Vogels, R., and Kovács, G. (2021). Evaluating the evidence for expectation suppression in the visual system. Neurosci. Biobehav. Rev. *126*, 368–381. https://doi.org/10.1016/j.neubiorev.2021.04.002.
9. Keysers, C., and Perrett, D.I. (2004). Demystifying social cognition: a Hebbian perspective. Trends Cognit. Sci. *8*, 501–507. https://doi.org/10.1016/j.tics.2004.09.005.
10. Keysers, C., and Gazzola, V. (2014). Hebbian learning and predictive mirror neurons for actions, sensations and emotions. Philos. Trans. R. Soc. Lond. B Biol. Sci. *369*, 20130175. https://doi.org/10.1098/rstb.2013.0175.
11. Keysers, C., Perrett, D.I., and Gazzola, V. (2014). Hebbian Learning is about contingency, not contiguity, and explains the emergence of predictive mirror neurons. Behav. Brain Sci. *37*, 205–206. https://doi.org/10.1017/S0140525X13002343.
12. Friston, K., Mattout, J., and Kilner, J. (2011). Action understanding and active inference. Biol. Cybern. *104*, 137–160. https://doi.org/10.1007/s00422-011-0424-z.
13. Kilner, J.M., Friston, K.J., and Frith, C.D. (2007). Predictive coding: an account of the mirror neuron system. Cognit. Process. *8*, 159–166. https://doi.org/10.1007/s10339-007-0170-2.
14. Bonini, L., Rozzi, S., Serventi, F.U., Simone, L., Ferrari, P.F., and Fogassi, L. (2010). Ventral premotor and inferior parietal cortices make distinct contribution to action organization and intention understanding. Cerebr. Cortex *20*, 1372–1385. https://doi.org/10.1093/cercor/bhp200.
15. Keysers, C., Kohler, E., Umiltà, M.A., Nanetti, L., Fogassi, L., and Gallese, V. (2003). Audiovisual mirror neurons and action recognition. Exp. Brain Res. *153*, 628–636. https://doi.org/10.1007/s00221-003-1603-5.
16. Kohler, E., Keysers, C., Umiltà, M.A., Fogassi, L., Gallese, V., and Rizzolatti, G. (2002). Hearing sounds, understanding actions: action representation in mirror neurons. Science *297*, 846–848. https://doi.org/10.1126/science.1070311.
17. Maranesi, M., Livi, A., Fogassi, L., Rizzolatti, G., and Bonini, L. (2014). Mirror neuron activation prior to action observation in a predictable context. J. Neurosci. *34*, 14827–14832. https://doi.org/10.1523/JNEUROSCI.2705-14.2014.
18. Umiltà, M.A., Kohler, E., Gallese, V., Fogassi, L., Fadiga, L., Keysers, C., Rizzolatti, G., Umilta, M.A., Kohler, E., Gallese, V., et al. (2001). I know what you are doing. a neurophysiological study. Neuron *31*, 155–165.
19. Ferroni, C.G., Albertini, D., Lanzilotto, M., Livi, A., Maranesi, M., and Bonini, L. (2021). Local and system mechanisms for action execution and observation in parietal and premotor cortices. Curr. Biol. *31*, 2819–2830.e4. https://doi.org/10.1016/j.cub.2021.04.034.
20. Thomas, R.M., De Sanctis, T., Gazzola, V., and Keysers, C. (2018). Where and how our brain represents the temporal structure of observed action. Neuroimage *183*, 677–697. https://doi.org/10.1016/j.neuroimage.2018.08.056.
21. Kilner, J.M., Vargas, C., Duval, S., Blakemore, S.-J., and Sirigu, A. (2004). Motor activation prior to observation of a predicted movement. Nat. Neurosci. *7*, 1299–1301. https://doi.org/10.1038/nn1355.
22. Smith, S.M., Miller, K.L., Salimi-Khorshidi, G., Webster, M., Beckmann, C.F., Nichols, T.E., Ramsey, J.D., and Woolrich, M.W. (2011). Network modelling methods for FMRI. Neuroimage *54*, 875–891. https://doi.org/10.1016/j.neuroimage.2010.08.063.
23. Schippers, M.B., and Keysers, C. (2011). Mapping the flow of information within the putative mirror neuron system during gesture observation. Neuroimage *57*, 37–44. https://doi.org/10.1016/j.neuroimage.2011.02.018.
24. Urgen, B.A., and Saygin, A.P. (2020). Predictive processing account of action perception: Evidence from effective connectivity in the action observation network. Cortex *128*, 132–142. https://doi.org/10.1016/j.cortex.2020.03.014.
25. Lerner, Y., Honey, C.J., Silbert, L.J., and Hasson, U. (2011). Topographic mapping of a hierarchy of temporal receptive windows using a narrated story. J. Neurosci. *31*, 2906–2915. https://doi.org/10.1523/JNEUROSCI.3684-10.2011.
26. Honey, C.J., Thesen, T., Donner, T.H., Silbert, L.J., Carlson, C.E., Devinsky, O., Doyle, W.K., Rubin, N., Heeger, D.J., and Hasson, U. (2012). Slow Cortical Dynamics and the Accumulation of Information over Long Timescales. Neuron *76*, 423–434. https://doi.org/10.1016/j.neuron.2012.08.011.
27. Cerliani, L., Bhandari, R., De Angelis, L., van der Zwaag, W., Bazin, P.-L., Gazzola, V., and Keysers, C. (2022). Predictive coding during action observation - A depth-resolved intersubject functional correlation study at 7T. Cortex *148*, 121–138. https://doi.org/10.1016/j.cortex.2021.12.008.
28. Finn, E.S., Huber, L., and Bandettini, P.A. (2021). Higher and deeper: Bringing layer fMRI to association cortex. Prog. Neurobiol. *207*, 101930. https://doi.org/10.1016/j.pneurobio.2020.101930.
29. Fries, P. (2015). Rhythms for Cognition: Communication through Coherence. Neuron *88*, 220–235. https://doi.org/10.1016/j.neuron.2015.09.034.
30. Bastos, A.M., Vezoli, J., and Fries, P. (2015). Communication through coherence with inter-areal delays. Curr. Opin. Neurobiol. *31*, 173–180. https://doi.org/10.1016/j.conb.2014.11.001.
31. Cannon, J., McCarthy, M.M., Lee, S., Lee, J., Börgers, C., Whittington, M.A., and Kopell, N. (2014). Neurosystems: brain rhythms and cognitive processing. Eur. J. Neurosci. *39*, 705–719. https://doi.org/10.1111/ejn.12453.
32. Stoll, F.M., Wilson, C.R.E., Faraut, M.C.M., Vezoli, J., Knoblauch, K., and Procyk, E. (2016). The Effects of Cognitive Control and Time on Frontal

Beta Oscillations. Cerebr. Cortex *26*, 1715–1732. https://doi.org/10.1093/cercor/bhv006.

33. Mooshagian, E., Holmes, C.D., and Snyder, L.H. (2021). Local field potentials in the parietal reach region reveal mechanisms of bimanual coordination. Nat. Commun. *12*, 2514. https://doi.org/10.1038/s41467-021-22701-3.
34. Tia, B., Takemi, M., Kosugi, A., Castagnola, E., Ansaldo, A., Nakamura, T., Ricci, D., Ushiba, J., Fadiga, L., and Iriki, A. (2017). Cortical control of object-specific grasp relies on adjustments of both activity and effective connectivity: a common marmoset study. J. Physiol. *595*, 7203–7221. https://doi.org/10.1113/JP274629.
35. Bastos, A.M., Vezoli, J., Bosman, C.A., Schoffelen, J.-M., Oostenveld, R., Dowdall, J.R., De Weerd, P., Kennedy, H., and Fries, P. (2015). Visual Areas Exert Feedforward and Feedback Influences through Distinct Frequency Channels. Neuron *85*, 390–401. https://doi.org/10.1016/j.neuron.2014.12.018.
36. Engel, A.K., and Fries, P. (2010). Beta-band oscillations—signalling the status quo? Curr. Opin. Neurobiol. *20*, 156–165. https://doi.org/10.1016/j.conb.2010.02.015.
37. Barone, J., and Rossiter, H.E. (2021). Understanding the Role of Sensorimotor Beta Oscillations. Front. Syst. Neurosci. *15*, 655886. https://doi.org/10.3389/fnsys.2021.655886.
38. Babiloni, C., Del Percio, C., Vecchio, F., Sebastiano, F., Di Gennaro, G., Quarato, P.P., Morace, R., Pavone, L., Soricelli, A., Noce, G., et al. (2016). Alpha, beta and gamma electrocorticographic rhythms in somatosensory, motor, premotor and prefrontal cortical areas differ in movement execution and observation in humans. Clin. Neurophysiol. *127*, 641–654. https://doi.org/10.1016/j.clinph.2015.04.068.
39. Moreno, I., de Vega, M., and León, I. (2013). Understanding action language modulates oscillatory mu and beta rhythms in the same way as observing actions. Brain Cognit. *82*, 236–242. https://doi.org/10.1016/j.bandc.2013.04.010.
40. Muthukumaraswamy, S.D., and Johnson, B.W. (2004). Primary motor cortex activation during action observation revealed by wavelet analysis of the EEG. Clin. Neurophysiol. *115*, 1760–1766. https://doi.org/10.1016/j.clinph.2004.03.004.
41. Simon, S., and Mukamel, R. (2016). Power modulation of electroencephalogram mu and beta frequency depends on perceived level of observed actions. Brain Behav. *6*, e00494. https://doi.org/10.1002/brb3.494.
42. Kilner, J.M., and Frith, C.D. (2008). Action observation: inferring intentions without mirror neurons. Curr. Biol. *18*, R32–R33. https://doi.org/10.1016/j.cub.2007.11.008.
43. Cerliani, L., Bhandari, R., De Angelis, L., van der Zwaag, W., Bazin, P.-L., Gazzola, V., and Keysers, C. (2021). Predictive coding during action observation - a depth-resolved intersubject functional correlation study at 7T. Preprint at bioRxiv. https://doi.org/10.1101/2021.08.30.458143.
44. Khanna, P., and Carmena, J.M. (2015). Neural oscillations: beta band activity across motor networks. Curr. Opin. Neurobiol. *32*, 60–67. https://doi.org/10.1016/j.conb.2014.11.010.
45. van Kerkoerle, T., Self, M.W., Dagnino, B., Gariel-Mathis, M.-A., Poort, J., van der Togt, C., and Roelfsema, P.R. (2014). Alpha and gamma oscillations characterize feedback and feedforward processing in monkey visual cortex. Proc. Natl. Acad. Sci. USA *111*, 14332–14341. https://doi.org/10.1073/pnas.1402773111.
46. Aggarwal, A., Brennan, C., Luo, J., Chung, H., Contreras, D., Kelz, M.B., and Proekt, A. (2022). Visual evoked feedforward-feedback traveling waves organize neural activity across the cortical hierarchy in mice. Nat. Commun. *13*, 4754. https://doi.org/10.1038/s41467-022-32378-x.
47. Bartoli, E., Bosking, W., and Foster, B.L. (2020). Seeing Visual Gamma Oscillations in a New Light. Trends Cognit. Sci. *24*, 501–503. https://doi.org/10.1016/j.tics.2020.03.009.
48. Brunet, N., Bosman, C.A., Roberts, M., Oostenveld, R., Womelsdorf, T., De Weerd, P., and Fries, P. (2015). Visual Cortical Gamma-Band Activity During Free Viewing of Natural Images. Cerebr. Cortex *25*, 918–926. https://doi.org/10.1093/cercor/bht280.
49. Maranesi, M., Livi, A., and Bonini, L. (2017). Spatial and viewpoint selectivity for others' observed actions in monkey ventral premotor mirror neurons. Sci. Rep. *7*, 8231. https://doi.org/10.1038/s41598-017-08956-1.
50. Caggiano, V., Fleischer, F., Pomper, J.K., Giese, M.A., and Thier, P. (2016). Mirror Neurons in Monkey Premotor Area F5 Show Tuning for Critical Features of Visual Causality Perception. Curr. Biol. *26*, 3077–3082. https://doi.org/10.1016/j.cub.2016.10.007.
51. Richter, C.G., Thompson, W.H., Bosman, C.A., and Fries, P. (2017). Top-Down Beta Enhances Bottom-Up Gamma. J. Neurosci. *37*, 6698–6711. https://doi.org/10.1523/JNEUROSCI.3771-16.2017.
52. Kopell, N., Ermentrout, G.B., Whittington, M.A., and Traub, R.D. (2000). Gamma rhythms and beta rhythms have different synchronization properties. Proc. Natl. Acad. Sci. USA *97*, 1867–1872. https://doi.org/10.1073/pnas.97.4.1867.
53. Ray, S., and Maunsell, J.H.R. (2011). Different origins of gamma rhythm and high-gamma activity in macaque visual cortex. PLoS Biol. *9*, e1000610. https://doi.org/10.1371/journal.pbio.1000610.
54. De Vries, I.E.J., and Wurm, M.F. (2022). Predictive neural representations of naturalistic dynamic input. Neuroscience *14*, 3858. https://doi.org/10.1101/2022.09.02.506366.
55. Rao, H.M., Mayo, J.P., and Sommer, M.A. (2016). Circuits for presaccadic visual remapping. J. Neurophysiol. *116*, 2624–2636. https://doi.org/10.1152/jn.00182.2016.
56. Zirnsak, M., and Moore, T. (2014). Saccades and shifting receptive fields: anticipating consequences or selecting targets? Trends Cognit. Sci. *18*, 621–628. https://doi.org/10.1016/j.tics.2014.10.002.
57. Schippers, M.B., Renken, R., and Keysers, C. (2011). The effect of intra- and inter-subject variability of hemodynamic responses on group level Granger causality analyses. Neuroimage *57*, 22–36. https://doi.org/10.1016/j.neuroimage.2011.02.008.
58. Walsh, K.S., McGovern, D.P., Clark, A., and O'Connell, R.G. (2020). Evaluating the neurophysiological evidence for predictive processing as a model of perception. Ann. N. Y. Acad. Sci. *1464*, 242–268. https://doi.org/10.1111/nyas.14321.
59. Redcay, E., and Schilbach, L. (2019). Using second-person neuroscience to elucidate the mechanisms of social interaction. Nat. Rev. Neurosci. *20*, 495–505. https://doi.org/10.1038/s41583-019-0179-4.
60. Abdelgabar, A.R., Suttrup, J., Broersen, R., Bhandari, R., Picard, S., Keysers, C., De Zeeuw, C.I., and Gazzola, V. (2019). Action perception recruits the cerebellum and is impaired in patients with spinocerebellar ataxia. Brain *142*, 3791–3805. https://doi.org/10.1093/brain/awz337.
61. Stadler, W., Ott, D.V.M., Springer, A., Schubotz, R.I., Schütz-Bosbach, S., and Prinz, W. (2012). Repetitive TMS Suggests a Role of the Human Dorsal Premotor Cortex in Action Prediction. Front. Hum. Neurosci. *6*, 20. https://doi.org/10.3389/fnhum.2012.00020.
62. Ziehe, A., Krämer, N., Popescu, F., and Müller, K.-R. (2010). Comparison of Granger Causality and Phase Slope Index. J. Mach. Learn. Res. - Proc. Track *6*, 267–276.
63. Bastos, A.M., and Schoffelen, J.-M. (2015). A Tutorial Review of Functional Connectivity Analysis Methods and Their Interpretational Pitfalls. Front. Syst. Neurosci. *9*, 175. https://doi.org/10.3389/fnsys.2015.00175.
64. Chopra, R., Murthy, C.R., and Rangarajan, G. (2018). Statistical Tests for Detecting Granger Causality. IEEE Trans. Signal Process., 1. https://doi.org/10.1109/TSP.2018.2872004.
65. Saleh, I. (2014). fMRI resting state time series causality: comparison of Granger causality and phase slope index. Int. J. Res. Med. Sci. *2*, 47. https://doi.org/10.5455/2320-6012.ijrms201402010.
66. Witham, C.L., Riddle, C.N., Baker, M.R., and Baker, S.N. (2011). Contributions of descending and ascending pathways to corticomuscular coherence in humans: Descending and ascending corticomuscular

coherence. J. Physiol. *589*, 3789–3800. https://doi.org/10.1113/jphysiol.2011.211045.

67. Young, C.K., Ruan, M., and McNaughton, N. (2017). A Critical Assessment of Directed Connectivity Estimates with Artificially Imposed Causality in the Supramammillary-Septo-Hippocampal Circuit. Front. Syst. Neurosci. *11*, 72. https://doi.org/10.3389/fnsys.2017.00072.
68. Brovelli, A., Ding, M., Ledberg, A., Chen, Y., Nakamura, R., and Bressler, S.L. (2004). Beta oscillations in a large-scale sensorimotor cortical network: Directional influences revealed by Granger causality. Proc. Natl. Acad. Sci. USA *101*, 9849–9854. https://doi.org/10.1073/pnas.0308538101.
69. Oostenveld, R., Fries, P., Maris, E., and Schoffelen, J.-M. (2011). FieldTrip: Open source software for advanced analysis of MEG, EEG, and invasive electrophysiological data. Comput. Intell. Neurosci. *2011*, 156869. https://doi.org/10.1155/2011/156869.
70. Qin, C., Tan, Z., Pan, Y., Li, Y., Wang, L., Ren, L., Zhou, W., and Wang, L. (2017). Automatic and Precise Localization and Cortical Labeling of Subdural and Depth Intracranial Electrodes. Front. Neuroinf. *11*, 10. https://doi.org/10.3389/fninf.2017.00010.
71. Reuter, M., Schmansky, N.J., Rosas, H.D., and Fischl, B. (2012). Within-subject template estimation for unbiased longitudinal image analysis. Neuroimage *61*, 1402–1418. https://doi.org/10.1016/j.neuroimage.2012.02.084.
72. Friston, K.J. (2003). Statistical parametric mapping. Neurosci. Databases Pract. Guide, 237–250.
73. Soyman, E., Bruls, R., Ioumpa, K., Müller-Pinzler, L., Gallo, S., Qin, C., van Straaten, E.C.W., Self, M.W., Peters, J.C., Possel, J.K., et al. (2022). Intracranial human recordings reveal association between neural activity and perceived intensity for the pain of others in the insula. Elife *11*, e75197. https://doi.org/10.7554/eLife.75197.
74. Amunts, K., Schleicher, A., and Zilles, K. (2007). Cytoarchitecture of the cerebral cortex—More than localization. Neuroimage *37*, 1061–1065. https://doi.org/10.1016/j.neuroimage.2007.02.037.
75. Nolte, G., Ziehe, A., Nikulin, V.V., Schlögl, A., Krämer, N., Brismar, T., and Müller, K.R. (2008). Robustly Estimating the Flow Direction of Information in Complex Physical Systems. Phys. Rev. Lett. *100*, 234101. https://doi.org/10.1103/PhysRevLett.100.234101.
76. Dhamala, M., Rangarajan, G., and Ding, M. (2008). Analyzing information flow in brain networks with nonparametric Granger causality. Neuroimage *41*, 354–362. https://doi.org/10.1016/j.neuroimage.2008.02.020.
77. Knief, U., and Forstmeier, W. (2021). Violating the normality assumption may be the lesser of two evils. Behav. Res. Methods *53*, 2576–2590. https://doi.org/10.3758/s13428-021-01587-5.
78. Schielzeth, H., Dingemanse, N.J., Nakagawa, S., Westneat, D.F., Allegue, H., Teplitsky, C., Réale, D., Dochtermann, N.A., Garamszegi, L.Z., and Araya-Ajoy, Y.G. (2020). Robustness of linear mixed-effects models to violations of distributional assumptions. Methods Ecol. Evol. *11*, 1141–1152. https://doi.org/10.1111/2041-210X.13434.

STAR★METHODS

KEY RESOURCES TABLE

REAGENT or RESOURCE	SOURCE	IDENTIFIER
Deposited data		
Data reported in the paper	This paper	OSF: https://doi.org/10.17605/OSF.IO/4XJG7
ActionPredictionECoG (The code used to analyze the data in this paper)	This paper	Zenodo: https://doi.org/10.5281/zenodo.8409871
Experimental models: Organisms/strains		
Human: Epilepsy patients	Jichi Medical University Hospital	N/A
Software and algorithms		
MATLAB 2021a	Mathworks	https://www.mathworks.com/; RRID:SCR_001622
Presentation	Neurobehavioral Systems	https://www.neurobs.com; RRID:SCR_002521
Fieldtrip	Oostenveld et al.[69]	https://www.fieldtriptoolbox.org; RRID:SCR_004849
FIELD	Qin et al.[70]	https://www.frontiersin.org/articles/10.3389/fninf.2017.00010/full
Freesurfer 7.3.2	Reuter et al.[71]	https://surfer.nmr.mgh.harvard.edu; RRID:SCR_001847
SPM12	Friston et al.[72]	https://www.fil.ion.ucl.ac.uk/spm/software/spm12/; RRID:SCR_007037
Other		
Sony HXR-MC50	Sony Europe B.V.	https://pro.sony/en_GB/products/handheld-camcorders/hxr-mc50p
EEG-1200	Nihon Kohden, Japan	https://eu.nihonkohden.com/en/products/neurology/neurofax.html
ECoG electrodes	Unique Medical, Japan	UZN C1-04-04-10-1-B, https://www.unique-medical.jp/products/medical-electrode/eeg-mep-sep-uzn/
ECoG electrodes	Unique Medical, Japan	UZN C1-20-05-10-1-B, https://www.unique-medical.jp/products/medical-electrode/eeg-mep-sep-uzn/
ECoG electrodes	Unique Medical, Japan	UZN C1-40-08-10-2-B, https://www.unique-medical.jp/products/medical-electrode/eeg-mep-sep-uzn/
Thinkpad L520	Lenovo Corporation, China	https://pcsupport.lenovo.com/us/en/products/laptops-and-netbooks/thinkpad-l-series-laptops/thinkpad-l520
MAGNETOM Skyra	Siemens, Germany	https://www.siemens-healthineers.com/en-us/magnetic-resonance-imaging/3t-mri-scanner/magnetom-skyra
Aquilion TSX-101A	Toshiba, Japan	https://jp.medical.canon/News/PressRelease/Detail/12853-834
Aquilion Prime SP TSX-303B	Canon Medical Systems, Japan	https://global.medical.canon/products/computed-tomography/aquilion_primesp
SOMATOM Definition AS+	Siemens, Germany	https://www.siemens-healthineers.com/en-us/computed-tomography/ecoline-refurbished-systems/somatomdefinitionas

RESOURCE AVAILABILITY

Lead contact

Further information and requests for resources should be directed to and will be fulfilled by the Lead Contact Christian Keysers (c.keysers@nin.knaw.nl).

Materials availability

This study did not generate new unique reagents.

Data and code availability

- Data reported in the paper is available at OSF.
- The code used to analyze the data in this paper is in the Github repository.
- Any additional information required to reanalyze the data reported in this work paper is available from the lead contact upon request.

EXPERIMENTAL MODEL AND STUDY PARTICIPANT DETAILS

Ethics

This study was approved by the ethics committee at Jichi Medical University Hospital and registered in the UMIN Clinical Trial Registry (number UMIN000040073). All participants had mental capacity and gave written informed consent to participation.

Participants

Ten subjects with refractory epilepsy participated in this study (five males and five females, aged 18–39 years, mean = 27.3 years, standard deviation = 7.3; see Table S1 for the demographic features of patients). Subdural electrodes were placed to localize epileptic foci and examine the cognitive and motor functions of areas under the electrodes. Preoperative interviews with the patients and family members, and an examination of available medical records, did not reveal social or communicative deficits in the included patients. Epileptic activity was not recorded from the electrodes included in our regions of interest. Nine of the patients included also participated in a task to be reported in a different manuscript, in which participants reported on a trial-by-trial basis how much pain they perceive a person to experience in short movies of the person's hand being hit by a belt. This task is known to depend on a kinematic analysis of the movements of the hand.[73] Comparing the ratings of these 9 patients againsts those of an age and sex-matched control group revealed that our group of patients was within the normal range (the z-scores were normally distributed, Shapiro-Wilk, SW = 0.935, p = 0.529, and a one-sample t test against zero, mean(z) = 0.04, t(8) = -0.116, p = 0.91, BF_{10} = 0.323) suggesting that their ability to perceive the kinematics of biological agents is preserved.

METHOD DETAILS

Stimuli and experiment procedure

The stimuli used here were a subset of those used in.[20] Briefly, twenty movies containing different daily actions (e.g., preparing sandwiches with butter and jam; see Table 1 for the full list) were simultaneously recorded by two video cameras (Sony MC50, 29 frames/s) at an angle of 45°. The videos were edited using Adobe Premiere ProCS5 running on Windows. Each movie was subdivided into shots containing one meaningful motor act each (e.g., taking bread, opening the butter dish, scooping butter with a knife, etc.). This was done on recordings from both camera angles. These motor acts (mean/standard deviation duration 2s ± 1s) were then assembled to build two types of ~1 min long stimuli (average 67s, Figure 1). For the Intact (I) presentation, the natural temporal sequence in which the acts were recorded was maintained, but a camera angle change was introduced between every two consecutive acts by alternate sampling from the recordings of the two cameras. In the Scrambled (S) versions, the acts remained the same, but the order of the acts was randomly re-arranged, and a camera angle change was introduced between every two consecutive acts. Camera angle changes were imposed at each act transition in both types of movies to compensate for the visual transients that would otherwise be present only in the scrambled movies. Because that stimulus set depicted actions typical for western Europeans, but the experiment was performed in Japan, author YO examined all twenty movies and selected 12 actions that should be familiar to Japanese participants (Table 1). This resulted in 12 intact and 12 scrambled movies. Each movie was presented twice. The experiment was conducted in 6 sessions. They were composed of 3 unique sessions presented twice, with each of the sessions including 4 intact and 4 scrambled movies presented in pseudorandom order, with an inter-movie interval between 8 and 12 s. No behavioral response was required during the experiment, but participants were to carefully observe the videos. Among the included participants, one completed only 3 sessions and one completed only 2 sessions.

Electrophysiological recordings and signal preprocessing

Intracranial EEG signals were recorded using a Nihon-Kohden system with 1000Hz sampling rate in Jichi Medical University Hospital, Japan. All signals were online referenced to two electrodes in the first head stage. All data analysis was conducted in MATLAB using the fieldtrip toolbox (www.fieldtriptoolbox.org/) and customized scripts. The recorded signals were first low-pass filtered using a 4th order Butterworth filter with a cutoff frequency at 200 Hz. The 50Hz power line noise and its harmonics were removed using bandstop filters with variable bandwidth according to individual power spectra. Channels with obvious artifacts were excluded from further

analysis. Each electrode was then locally re-referenced to the average of its neighboring electrodes within 12mm spatial distance. This procedure removes the common recording reference, which otherwise leads to spurious correlations and coherence. Coherence, imaginary coherence, phase-slope index and Granger causality were exclusively calculated between electrodes, for which the neighboring electrodes used for re-referencing had no overlap. Data were down-sampled to 500 Hz for subsequent analyses.

Electrode locations and region definition

The spatial locations were derived from each patient's pre-implantation MR images and post-implantation CT images. For each patient, the post-implantation CT was co-registered to the pre-implantation MRI using a six-parameter rigid body transformation, implemented in SPM12 (https://www.fil.ion.ucl.ac.uk/spm/software/spm12/). The registration was visually verified and manually adjusted if necessary. ECoG electrodes were identified semi automatically according to anatomical landmarks in native space.[70] For visualization of all subjects' electrodes on an average surface, individual electrode coordinates were transformed to MNI152 space using the Freesurfer CVS function(v6.0.0, surfer.nmr.mgh.harvard.edu/). The regions of interest including precentral gyrus (PreCG), supramarginal gyrus (SMG) and middle occipital gyrus (MOG) were extracted from the Anatomy toolbox[74](Figure 1C).

Trial separation

In the connectivity analysis including coherence, phase slope index and granger causality, data were first separated into trials based on the time of the camera change. The actions used in our stimuli were composed of a sequence of different shorter acts (e.g., the action of buttering bread included the acts of e.g., taking bread, opening the butter dish, scooping butter with a knife, etc.). These acts were used as ''action primitives'' and determined the location of the camera changes. The intervals between two camera changes therefore depended by the duration of each act, and varied from 0.4–6.76s. In our analyses, to minimize the overlap between trials as well as preserving the temporal dynamics during action perception, we thus chose a time window from −0.5s to 1s relative to the camera change.

QUANTIFICATION AND STATISTICAL ANALYSIS

Power spectral density

Power spectral density was estimated from 2 to 120Hz using the ft_freqanalysis function, and separate parameters for low (2-30Hz) and high frequencies (30-120Hz). For the low frequencies, the power spectrum was estimated by a short-time Fourier transform with Hann tapers of 1s, sliding over the whole experimental session in steps of 0.1s and averaged over all windows in a given condition. For the high-frequency part, we used a multi-taper spectral estimation with 5 tapers in 0.5s windows sliding in steps of 0.1s, and results were also averaged over all time windows in a given condition. Power difference between conditions in each frequency was then compared using all the electrodes in each selected region of interest (Figure 2). In some analyses, we used *a priori* bands of interest in order to compare the power difference for specific frequency bands: we averaged the power from 20 to 30Hz for the high-beta band and from 60 to 90Hz for the gamma band in both Intact (I) and Scrambled (S) conditions for each subject (Figure 2 inset; Figure 3).The raw power of each frequency was multiplied by the square of frequency for better visualization in Figure 2.

Coherence

For the selected time window, all trial data in each electrode within this window were Fourier transformed using multi-tapering with 6Hz frequency smoothing in frequencies ranging from 2 to 120Hz with 1Hz step using ft_freqanalysis. The coherence between two signals was then calculated in each electrode pair and each region pair in both conditions using ft_connectivityanalysis, the imaginary part of coherence was taken as the metric to measure the synchronization between regions (Figures 4A and 4B). The time-resolved coherence was calculated in a sliding-window manner with window length of 1 s and steps of 0.1s and averaged across the frequency points in each frequency band of interest (Figures 4C and 4D).

Phase slope index

The phase slope index (PSI) was calculated in a similar manner as coherence across regions.[75] All trial data for each electrode were Fourier transformed using multi-tapering with 4Hz frequency smoothing and 1Hz frequency resolution. The phase slope index was then calculated ft_connectivityanalysis across frequencies ranging from 20 to 30Hz and 60 to 90Hz with the same bandwidth of 4Hz for each frequency; the PSI values were then averaged, separately for each of the two frequency bands, to get the temporal dynamics, this was done in each electrode pair for each region pair in both conditions as well (Figure 6).

Granger causality

Granger causality (GC) was calculated in a time window from 0 to 1s relative to the camera change using the nonparametric estimation.[68,76] The Fourier spectrum was estimated using the same parameters as the PSI mentioned above and entered into a nonparametric spectral matrix factorization as implemented in the Fieldtrip toolbox[69] (Figure 5).

Statistical assessment

Statistical assessments were performed to compare the difference between conditions using the LME model implemented in MATLAB. We implemented the LME model with patient and electrode (or electrode pairs) as two random effects and used the restricted maximum likelihood method to optimize. In the model, fixed and random effects were considered together. Post hoc tests of p values were performed using FDR correction to correct for multiple comparisons not specified otherwise. Statistical inferences were under a significance threshold of $p < 0.05$ if not specified otherwise. As there is no non-parametric alternative to LME that could accommodate the nested structure of our data, and as LME has been shown to be robust against violation of normality,[77,78] we did not test our residuals for normality.